Research Square

Preprints are preliminary reports that have not undergone peer review.
They should not be considered conclusive, used to inform clinical practice,
or referenced by the media as validated information.

Is the Matanomadh Jarosite Occurrence Supergene or Hydrothermal? A Regional Stream-Sediment Geochemical Test, Kachchh Basin, Western India

Sneha Bhaumik
Geological Survey of India
Sreemoyee Chakraborty
sreemoyee93@gmail.com

Blue Blocks Micro Research Institute https://orcid.org/0000-0001-5180-156X
Saptarshi Mallick
Geological Survey of India
Sreejata Sarkar
Geological Survey of India
Arup Ratan Manna
Geological Survey of India
Asthajita Bhuyan
Krantiguru Shyamji Krishna Verma Kachchh University
Kalyan Kumar Neog
Krantiguru Shyamji Krishna Verma Kachchh University
Rosalin Das
Fakir Mohan University
Jayaprakash Mahakul
Geological Survey of India
Satyananda Maiti
Geological Survey of India
Bhoomika Mod
Krantiguru Shyamji Krishna Verma Kachchh University

Research Article

Keywords: Matanomadh, jarosite, Kachchh Basin, Mars analog, supergene weathering, stream-sediment geochemistry, principal component analysis, factor analysis, pathfinder elements

Posted Date: October 28th, 2026

DOI: https://doi.org/10.21203/rs.3.rs-11520013/v1

License: This work is licensed under a Creative Commons Attribution 4.0 International License.
Read Full License

Additional Declarations: The authors declare no competing interests.

Is the Matanomadh Jarosite Occurrence Supergene or Hydrothermal? A Regional Stream-Sediment Geochemical Test, Kachchh Basin, Western India

Sneha Bhaumik [1, 2, *], Sreemoyee Chakraborty[3], Saptarshi Mallick[4], Sreejata Sarkar[2], Arup Ratan Manna[2], Asthajita Bhuyan[5], Kalyan Kumar Neog[5], Rosalin Das[1], Jayaprakash Mahakul[2], Satyananda Maiti[2], Bhoomika Mod[5]

[1] *Department of Geology, Fakir Mohan University, Balasore 756 089, India*
[2]*Geological Survey of India, State Unit: Odisha, Bhubaneswar 751 012, India*
[3] *Blue Blocks Micro Research Institute, Hyderabad 500 032, India*
[4]*Geological Survey of India, State Unit: Meghalaya, Shillong 793006, India*
[5] *Department of Geology, K.S.K.V. Kachchh University, Bhuj, Gujarat 370 001, India*
**Corresponding author: sneha.bhaumik@gsi.gov.in*

Conference Paper presented at the 42nd Convention of the Indian Association of Sedimentologists, hosted by the Department of Geological Sciences, Gauhati University

Abstract

The jarosite occurrence at Matanomadh, Kachchh Basin, western India, hosted within the Paleocene Matanomadh Formation overlying weathered Deccan Trap basalt, has attracted sustained mineralogical, spectroscopic, and stable-isotope attention as a terrestrial Mars analog, yet its genetic timing and mechanism remain debated: some workers have proposed that the mineral assemblage records an ancient, possibly volcanogenic-hydrothermal, Paleocene acid-sulfate paleoenvironment, while the most recent multiproxy (XRD–XRF–FTIR–Raman–$\delta^{34}S$) study interprets jarosite formation across the western Kutch succession as an ongoing, low-temperature process driven by supergene pyrite oxidation. All of this prior work, however, has characterized the occurrence at outcrop and hand-sample scale, without reference to the surrounding basin's regional geochemical framework. This study addresses that gap by testing whether the trace- and pathfinder-element geochemistry of the jarosite-bearing domain (n = 30, comprising an initial 15 samples analysed for Fe_2O_3, SO_3, K_2O, Al_2O_3, Mo, As, U, and Th, and a further 15 samples additionally analysed for SiO_2, Sb, Se, Pb, Cu, and Zr) is embedded within, or decoupled from, the detrital provenance and hydrothermal-affinity framework established independently from a 1,295-sample, 58-variable regional stream-sediment geochemical survey of the Kachchh Mainland. Multivariate analysis of the

regional dataset (Kaiser–Meyer–Olkin = 0.880; Bartlett's χ^2 = 120,039.46, $p < 0.001$) resolved 12 significant principal components (77.47% of variance) and an eight-factor Varimax solution dominated by a detrital REE–U–Hf–Zr–Ta provenance signature (Factor 1) and a silica-versus-mafic lithological contrast (Factor 2), with subordinate potassic/hydrothermal (Rb–K_2O–Ba–Li–W; Factor 4) and Ti–Cr–Mo (Factor 6) associations. Relative to the geochemistry of the 20 nearest regional stream-sediment samples, the jarosite domain is strongly enriched in Fe_2O_3 (≈ 4.9× local median), K_2O (≈ 3.8×), Mo (≈ 19.1×), As (≈ 3.1×), Sb (≈ 39.6×), Se (≈ 34.0×), Pb (≈ 2.7×), and Cu (≈ 2.1×), but is depleted in Al_2O_3 (≈ 0.55×), SiO_2 (≈ 0.20×), and, most diagnostically, Th (≈ 0.06×) and Zr (≈ 0.04× , both roughly one to two orders of magnitude below local background), and shows no enrichment in U relative to background (≈ 0.99×). This pattern indicates that the jarosite domain does not inherit the region's dominant detrital REE–Th–Zr provenance signature or its bulk quartzo-feldspathic sediment character, and is compositionally decoupled from the basin's principal lithological framework, consistent with an authigenic, in-situ Fe–S–K mineral phase rather than a reworked fragment of regional detritus; the coupled Mo–As–Sb–Se–Pb–Cu enrichment is consistent with pathfinder- and chalcophile-element scavenging during low-temperature Fe(III)-oxyhydroxysulfate precipitation, and the elevated K_2O is more parsimoniously explained by the jarosite crystal structure itself than by the region's independent potassic-hydrothermal factor. Together, these basin-scale geochemical observations provide an independent line of evidence consistent with the recently proposed ongoing supergene, pyrite-oxidation-driven origin of the Matanomadh jarosite, complementing the isotopic and mineralogical case built at outcrop scale, and they illustrate a transferable regional-versus-local geochemical framework for testing the origin of comparable secondary-mineral anomalies elsewhere in the Kachchh Basin.

Keywords: Matanomadh; jarosite; Kachchh Basin; Mars analog; supergene weathering; stream-sediment geochemistry; principal component analysis; factor analysis; pathfinder elements

1. Introduction

Jarosite [$KFe_3(SO_4)_2(OH)_6$] is a low-temperature Fe–K sulfate mineral that forms almost exclusively under acidic, highly oxidizing, sulfate-rich conditions, and its identification on the surface of Mars by the Opportunity rover at Meridiani Planum established it as a key mineralogical indicator of past aqueous, acidic environments on that planet (Farrand et al., 2009; Guha et al., 2026). Because comparable terrestrial jarosite occurrences are geologically accessible and can be studied in far greater analytical detail than their Martian counterparts, they have become important “Mars analog” field laboratories for understanding the range of conditions under which jarosite can form and persist (Bhattacharya et al., 2016). The Matanomadh area of the Kachchh Basin, western India, hosts one of

the most extensively studied such localities: jarosite occurs within saprolitic clay horizons developed over weathered Deccan Trap basalt and within the overlying tuffaceous shale, sandstone, and clay units of the Paleocene Matanomadh Formation, commonly as secondary veins, gypsum-associated fracture fillings, and coatings on kaolinite clasts (Bhattacharya et al., 2016; Dharaiya et al., 2025). Despite this attention, the genetic timing and mechanism of the Matanomadh jarosite remain debated in the recent literature. Some workers have interpreted the assemblage jarosite together with alunite, kaolinite, gypsum, and goethite as a record of an ancient, Palaeocene acid-sulfate paleoenvironment, noting that the acidic conditions required for jarosite stability could conceivably have been "potentially driven by volcanic activity or hydrothermal processes during the Palaeocene" contemporaneous with, or shortly following, emplacement of the underlying Deccan Traps (Dharaiya et al., 2025). By contrast, the most recent and analytically comprehensive study of the western Kutch hydroxy-sulfate assemblage integrating XRD, XRF, FTIR, Raman spectroscopy, and stable sulfur-isotope ($\delta^{34}S$) analysis across multiple chronostratigraphic units from the pre-Deccan Ghuneri Member (Late Cretaceous) through the post-Deccan Matanomadh, Naredi, and Harudi formations concludes that jarosite formation in this region is an ongoing, low-temperature process driven by supergene oxidation of pre-existing sedimentary pyrite, rather than a fossil record of a single ancient hydrothermal event (Guha et al., 2026). Resolving this distinction matters beyond stratigraphy: a supergene, pyrite-oxidation origin implies that jarosite formation here is a contemporary near-surface weathering process with no necessary connection to buried mineralization, whereas a Paleocene volcanogenic-hydrothermal origin would carry different implications both for the paleoenvironmental record preserved at this Mars-analogue site and for the possible presence of an associated hydrothermal system in the surrounding basin.

All of the existing geochemical, mineralogical, and isotopic evidence for this debate, however, has been generated at outcrop and hand-sample scale, focused specifically on the jarosite-bearing horizon itself. None of the published studies has evaluated the Matanomadh occurrence against the broader geochemical framework of the surrounding Kachchh Mainland, even though a substantial regional stream-sediment geochemical dataset covering 1,295 samples and 58 major, trace, and rare-earth-element variables across the Kachchh Mainland, and encompassing the Matanomadh area within its sampling footprint already exists for this purpose. Regional stream-sediment geochemistry integrates the detrital and lithological signal of upstream catchments (Nazarpour et al., 2022; Rai et al., 2026) and, through multivariate methods such as Principal Component Analysis (PCA) and R-mode factor analysis, can resolve the dominant provenance, lithological, and hydrothermal-affinity associations that characterize a region (Reimann et al., 2002). If the Matanomadh jarosite domain's trace-element geochemistry is embedded within this regional detrital and hydrothermal-affinity

framework for example, if it inherits the region's dominant heavy-mineral/REE provenance signature, or if its potassium enrichment aligns with the region's independent potassic-hydrothermal geochemical factor this would lend support to a genetic connection with the region's broader lithological or hydrothermal history. Conversely, if the jarosite domain's geochemistry is decoupled from this regional framework, an authigenic, locally generated, low-temperature origin becomes the more parsimonious explanation.

This study therefore uses the existing 1,295-sample regional stream-sediment dataset to build an independent, basin-scale geochemical framework comprising correlation structure, PCA, and R-mode Varimax factor analysis and tests a 30-sample Matanomadh jarosite-domain geochemical dataset against it in two complementary ways: first, by comparing the jarosite domain directly with the geochemistry of the nearest regional stream-sediment samples (a local-background comparison), and second, by evaluating whether the jarosite domain's elemental associations align with, or are decoupled from, the region's principal detrital-provenance and hydrothermal-affinity factors.

The aim is not to duplicate the isotopic and mineralogical case already built for this locality, but to provide an independent, regional-scale geochemical line of evidence bearing on the same genetic question, and to demonstrate a transferable local-versus-regional geochemical framework that can be applied to other secondary-mineral anomalies within the Kachchh Basin.

A secondary aim of this study is to characterize the regional detrital, lithological, and hydrothermal-affinity geochemical structure of the Kachchh Mainland stream-sediment dataset in its own right, since this framework comprising a silica-versus-mafic lithological contrast, a resistant accessory-mineral/REE–U–Hf–Zr provenance signature, and several subordinate potassic-hydrothermal and Ti–Cr–Mo associations provides useful regional context for future geological and exploration studies in the basin independent of the jarosite question addressed here.

2. Regional and Local Geological Setting

2.1 Kachchh Basin

The Kachchh Basin of western India is a structurally complex, pericratonic rift basin developed along inherited Precambrian structural trends, recording a prolonged geological history from the Mesozoic to the Recent (Biswas, 2005; Mandal et al., 2023). The basin originated during the break-up of eastern Gondwanaland and is bounded by the Nagar Parkar uplift to the north and the Kathiawar (Saurashtra) uplift to the south; internally it is styled by three principal E–W-trending uplifts the Island Belt, Kachchh Mainland, and Wagad uplifts separated by intervening grabens and

half-grabens along major basement-involved faults (Biswas, 2005). The Mesozoic succession, exposed extensively across the Kachchh Mainland, comprises carbonate-, shale-, and sandstone-dominated formations (Jhurio, Jhumara, Jhuran, and Bhuj formations) deposited under changing marine to continental conditions. During the Late Cretaceous–Paleocene, extensive Deccan Trap volcanism introduced basaltic lava flows and associated intrusive bodies into the sedimentary succession, and the basin remains seismically active, as demonstrated by the 1819 Allah Bund and 2001 Bhuj earthquakes and by recent paleoseismological work along the Kachchh Mainland Fault (Malik et al., 2024).

2.2 The Matanomadh Formation and its jarosite occurrence

The Matanomadh Formation forms the basal unit of the Tertiary succession in the Kachchh Mainland, unconformably overlying a laterally extensive, lateritized post-Trappean surface developed on the Deccan Traps and disconformably underlying the lignite-bearing, early-to-middle Eocene Naredi Formation (Biswas, 1992; Srivastava and Singh, 2017; Chauhan et al., 2021). The formation is lithologically divisible into a lower Laterite Member, characterized by variegated laterite and kaolinitic clay, and an upper Clastic Member, characterized by tuffaceous shale, altered carbonaceous sandstone, and lignitic shale, deposited in a fluvial-to-estuarine or lagoonal setting under intermittently arid-to-semi-arid climatic conditions (Srivastava and Singh, 2017; Dharaiya et al., 2025). Jarosite at Matanomadh occurs both within the saprolitic clay horizons developed over the weathered basalt and within the overlying variegated sandstone, shale, and clay units of the Clastic Member, typically as secondary veins (with or without associated gypsum) and as coatings on kaolinite clasts, in association with Al-rich phyllosilicates (kaolinite) overlying a zone of Fe–Mg smectites in the altered basalt (Bhattacharya et al., 2016). Natroalunite has also been documented within the same saprolitic clay horizon (Chitale, 1987), and the most recent multiproxy study has extended the hydroxy-sulfate mineral assemblage (jarosite, alunite, minamiite, gypsum, and natrojarosite–natroalunite solid solutions) across multiple chronostratigraphic units of the western Kutch succession, from the pre-Deccan Ghuneri Member through the post-Deccan Matanomadh, Naredi, and Harudi formations (Guha et al., 2026).

This combination of features acidic, oxidizing, sulfate-rich secondary mineralization developed on weathered basalt and overlying tuffaceous clastic rocks under an arid-to-semi-arid paleoclimate , has been widely cited as analogous to the geological settings inferred for jarosite-bearing localities on Mars, such as Meridiani Planum and Mawrth Vallis (Bhattacharya et al., 2016; Farrand et al., 2009; Guha et al., 2026), and the Matanomadh site is now recognized as a geoheritage locality of international scientific significance for planetary-analog research (Chauhan et al., 2021). The stream-

sediment sample localities examined for the jarosite-domain geochemical dataset in the present study (centred near 23.54°N, 68.96°E) fall within the coordinate range reported for the Matanomadh jarosite occurrence in the recent literature (e.g., Dharaiya et al., 2025), and the present dataset is accordingly interpreted as sampling this same, or an immediately adjacent, jarosite-bearing domain within the Matanomadh Formation.

3. Materials and Methods

3.1 Sample datasets and analytical basis

Two complementary datasets are used in this study. The first is a regional stream-sediment geochemical dataset comprising 1,295 samples and 58 geochemical variables (major oxides, trace elements, and rare-earth elements) collected across the Kachchh Mainland, used here to establish the region's detrital, lithological, and hydrothermal-affinity geochemical framework. The second is a spatially discrete jarosite-domain dataset from Matanomadh (centred near 23.54°N, 68.96°E), assembled in two stages: an initial set of 15 samples (PM-JAR-01 to PM-JAR-15) analysed for Fe_2O_3, SO_3, K_2O, Al_2O_3, Mo, As, U, and Th, and a subsequent set of 15 additional samples from the same domain (PM-JAR-16 to PM-JAR-30) analysed by XRF for major oxides (including SiO_2) and by ICP-MS for an extended trace-element suite (Mo, As, Sb, Se, U, Th, Pb, Cu, and Zr). Combining both sets gives n = 30 for the eight variables common to both (Fe_2O_3, SO_3, K_2O, Al_2O_3, Mo, As, U, Th) and n = 15 (PM-JAR-16–30 only) for the six variables analysed only in the second stage (SiO_2, Sb, Se, Pb, Cu, Zr). [Authors: please insert here the sample-medium and mesh-fraction specification, the analytical laboratory for both stages, and a brief statement of quality assurance/quality control , certified reference materials, duplicate analyses, and detection limits , as these details are required by international geochemistry journals but were not present in the source materials supplied for this revision.]

3.2 Data screening and standardization

Prior to statistical analysis, the regional dataset was screened to exclude seven variables with no analytical variation (LOI, Pt, Pd, F, In, Tl, Te), retaining 58 variables for 1,295 complete samples. Because the analysed variables are reported in different units and concentration ranges, all variables were standardized to zero mean and unit standard deviation prior to PCA and factor analysis, a routine pre-processing step in multivariate geochemical exploration studies (Reimann et al., 2002).

3.3 Correlation analysis and sampling adequacy

Descriptive statistics and Pearson correlation coefficients were computed for all 58 retained variables. The suitability of the correlation matrix for dimension-reduction analysis was evaluated

using the Kaiser–Meyer–Olkin (KMO) measure of sampling adequacy and Bartlett's test of sphericity.

3.4 Principal Component Analysis

PCA was performed on the standardized regional geochemical variables. Components with eigenvalues greater than 1.0 (the Kaiser criterion) were retained for interpretation.

3.5 R-mode Exploratory Factor Analysis

R-mode Exploratory Factor Analysis (EFA) using principal-component extraction was applied to the regional dataset to resolve latent groups of variables with common variance, followed by orthogonal Varimax rotation with Kaiser normalization. Absolute rotated loadings ≥ 0.50 were treated as strong associations for interpretation, following common practice in R-mode factor-analytic studies of stream-sediment data (Shine et al., 2022; Helba et al., 2021; Rai et al., 2026).

3.6 Spatial anomaly mapping and PCA-based multivariate anomaly index

Single-element anomaly maps for thirteen major and trace elements were generated and overlain on the 1:25,000 geological map of the study area. A PCA-based multivariate anomaly index was additionally constructed from the PC1–PC2 score space: the radial (Euclidean) distance of each sample from the origin was used as a multivariate screening statistic, and samples within the upper 5% of this distance distribution (threshold = 7.98) were flagged as multivariate PCA anomalies.

3.7 Compositional-data considerations

Stream-sediment geochemical data are compositional, and this closure constrains the covariance structure of the raw data and can bias standard multivariate techniques if applied without an appropriate transformation (Aitchison, 1986; Filzmoser et al., 2009a, 2009b; Reimann et al., 2012). The principal regional analyses reported here (Sections 4.1–4.4) were performed on the standardized concentrations as supplied. A supplementary sensitivity analysis, in which all variables were converted to a common ppm basis, zero values were replaced using a multiplicative simple-replacement approach (Martin–Fernández et al., 2003), a centred log-ratio (clr) transformation was applied, and PCA was re-run, is reported in Section 5.4 to test the robustness of the regional factor structure to data closure.

3.8 Local-background comparison for the jarosite domain

To test the jarosite domain against its immediate geochemical surroundings rather than against basin-wide averages, the great-circle (haversine) distance from the centroid of the original 15 jarosite-

domain sample locations to every regional stream-sediment sample was computed, and the 20 nearest regional samples (all within 5.4 km of the jarosite-domain centroid) were extracted to define a local stream-sediment background; the same background set was used to benchmark the 15 additional PM-JAR-16–30 samples, which were collected from the same domain. For the eight variables common to both stages of the jarosite dataset and the regional survey (Fe_2O_3, K_2O, Al_2O_3, Mo, As, U, and Th, plus SO_3 which the regional survey did not measure), the combined n = 30 jarosite dataset was compared with the local background; for the six variables analysed only for PM-JAR-16–30 (SiO_2, Sb, Se, Pb, Cu, Zr), the n = 15 subset was compared with the same local background. In each case, a median-based enrichment/depletion factor (jarosite-domain median ÷ local-background median) was calculated. This comparison, together with the regional factor/PCA structure (Sections 3.4–3.5), was used to evaluate whether the jarosite domain's geochemistry is embedded within, or decoupled from, the region's dominant detrital-provenance and hydrothermal-affinity associations (Section 5.3).

4. Results

4.1 Regional descriptive statistics and correlation structure

Statistical analysis was performed on 1,295 complete regional samples and 58 geochemical variables. The correlation matrix demonstrates a strong, coherent structure among several groups of elements. The strongest positive correlations occur among the heavy and middle rare-earth elements, including Tb–Gd (r = 0.99), Tm–Yb (r = 0.99), Pr–Dy (r = 0.99), and Yb–Lu (r = 0.99), indicating highly coherent REE behaviour. Among the major elements, SiO_2 shows strong negative correlations with MgO (r = -0.78), Fe_2O_3 (r = -0.73), Al_2O_3 (r = -0.72), and CaO (r = -0.63), indicating an important compositional contrast between quartz-rich and Fe–Mg–Al/Ca-bearing sediment components (Fig. 1; Table 1).

This regional correlation structure provides the detrital/lithological backdrop against which the jarosite-domain geochemistry (Section 4.8) is tested in Sections 4.9 and 5.3.

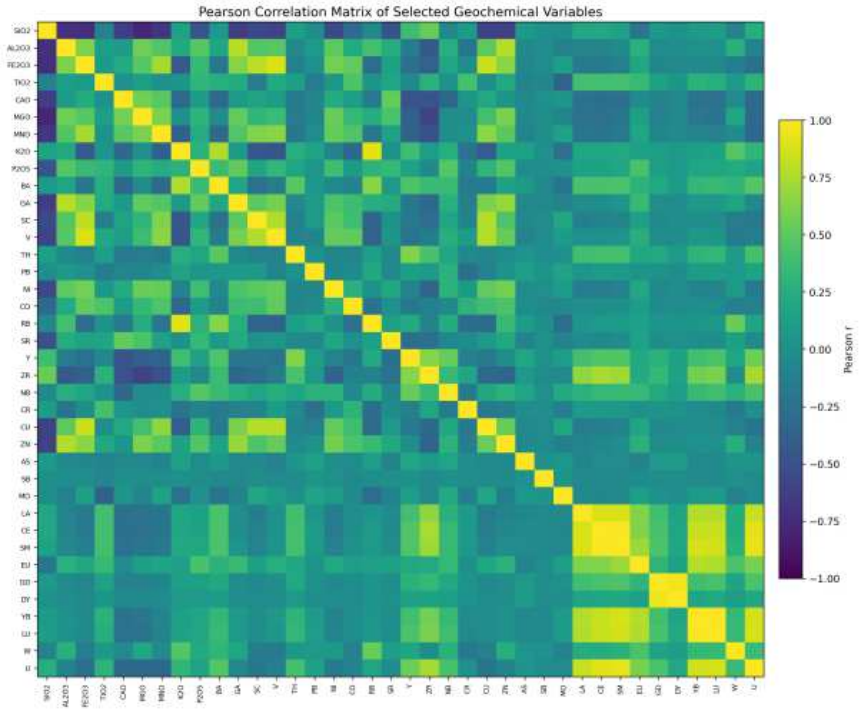


Fig. 1. Pearson correlation matrix for selected major, trace, and rare-earth-element variables of the regional stream-sediment dataset. Red/blue polarity represents positive/negative association, respectively.

Element pair	**r**	**Relationship**
Tb – Gd	0.994	Positive
Tm – Yb	0.994	Positive
Pr – Dy	0.992	Positive
Yb – Lu	0.991	Positive
Ce – Sm	0.989	Positive
Ho – Tm	0.988	Positive
SiO_2 – MgO	-0.780	Negative
SiO_2 – Fe_2O_3	-0.733	Negative
SiO_2 – Al_2O_3	-0.715	Negative
SiO_2 – MnO	-0.677	Negative
SiO_2 – Ga	-0.640	Negative
SiO_2 – CaO	-0.632	Negative

Table 1. Selected strongest positive and negative Pearson correlations among the analysed regional variables.

4.2 Sampling adequacy: KMO and Bartlett's test

The Kaiser–Meyer–Olkin (KMO) measure of sampling adequacy for the regional dataset was 0.880, and Bartlett's test of sphericity was highly significant (χ^2 = 120,039.46, df = 1653, $p < 0.001$), confirming that dimension-reduction methods are statistically justified.

4.3 Regional Principal Component Analysis

Twelve components have eigenvalues > 1 and collectively explain approximately 77.47% of total variance (Table 2; Fig. 2). PC1 accounts for 22.26% of variance and PC2 for 15.77%. The distribution of the regional samples in PC1–PC2 score space is shown in Fig. 3, and the variables contributing most strongly to the two components are shown in Fig. 4. PC1 is dominated by strong positive loadings of U (+0.93), the REE assemblage, and Zr (+0.74), consistent with a resistant accessory-mineral and provenance control. PC2 is dominated by a strong positive SiO_2 loading (+0.85) contrasted against negative loadings of Al_2O_3 (-0.82), Fe_2O_3 (-0.81), Zn (-0.80), MgO (-0.72), and Ni (-0.67), reflecting the silica-rich versus Fe–Mg-rich lithological contrast that also emerges as Factor 2 in the Varimax solution.

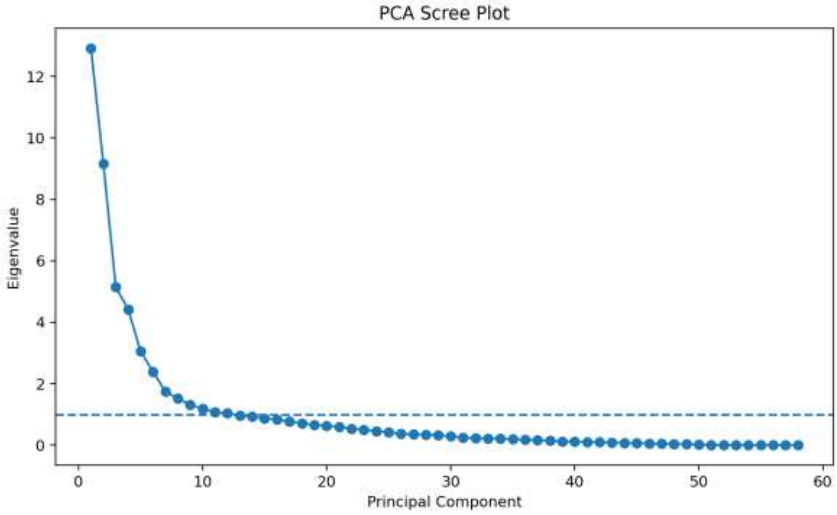


Fig. 2. PCA scree plot for the regional dataset.

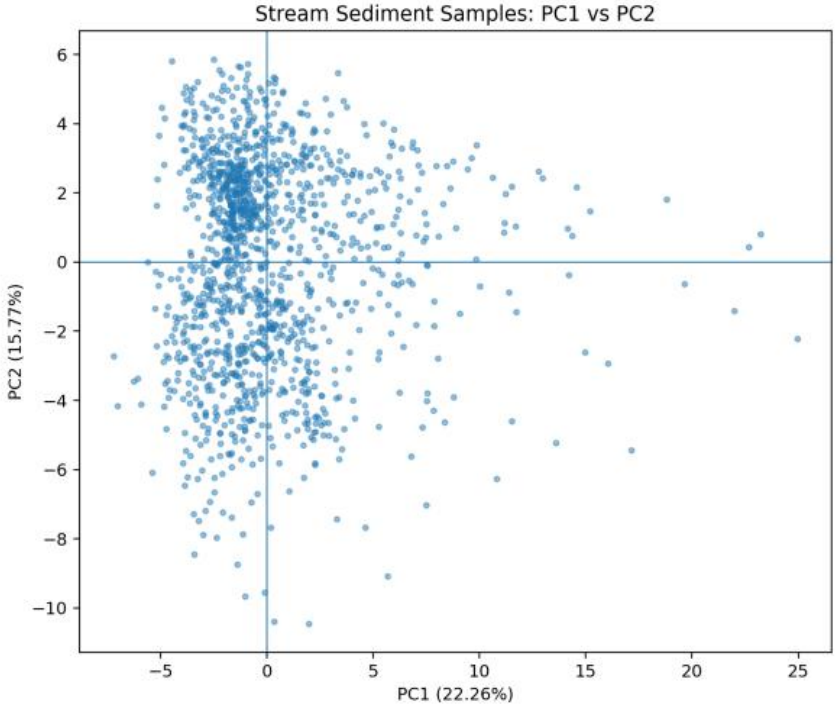


Fig. 3. PCA score plot showing the distribution of regional stream-sediment samples along PC1 and PC2.

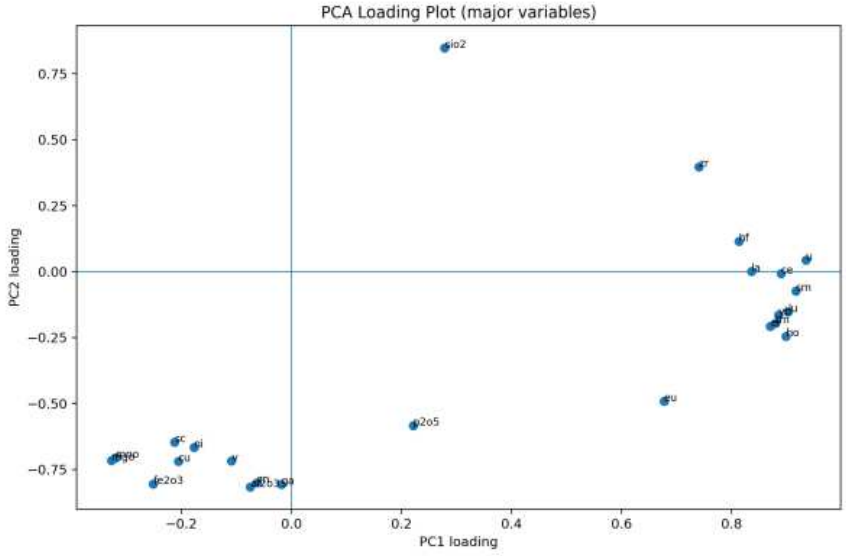


Fig. 4. PCA loading plot showing variables with the strongest contributions to PC1 and PC2.

Component	Eigenvalue	Variance (%)	Cumulative (%)	Retain
1	12.919	22.26	22.26	Yes
2	9.154	15.77	38.03	Yes
3	5.145	8.86	46.89	Yes
4	4.417	7.61	54.50	Yes
5	3.058	5.27	59.77	Yes
6	2.389	4.12	63.88	Yes
7	1.749	3.01	66.90	Yes
8	1.522	2.62	69.52	Yes
9	1.322	2.28	71.80	Yes
10	1.182	2.04	73.83	Yes
11	1.072	1.85	75.68	Yes
12	1.037	1.79	77.47	Yes
13–23	0.509–0.962	0.88–1.66	79.12–91.27	No

Table 2. Regional PCA eigenvalues and explained variance (rows 13–23 condensed; full table available on request).

4.4 Regional R-mode Factor Analysis and Varimax rotation

An eight-factor Varimax solution was retained for the regional dataset. The rotated loadings of Factors 1 and 2 are plotted in Fig. 5, the full eight-factor loading structure is summarised as a heatmap in Fig. 6, and the proportion of variance carried by each factor is shown in Fig. 7. For interpretation, absolute rotated loadings ≥ 0.50 were treated as strong associations. Factor 1 is dominated by the heavy-to-light REE suite (Yb, Ho, Tm, Lu, Sm, Ce, La, Eu, Er) together with U, Hf, Zr, and Ta , the region's principal detrital, resistant accessory-mineral provenance signature. Factor 2 (Fe_2O_3, V, Cu, Sc, Ga, Zn, Al_2O_3, MnO, Ni, and MgO, all negative, opposed by positive SiO_2) represents the silica-rich versus Fe–Mg-rich lithological contrast. Factor 3 is a second, geochemically distinct REE-related factor, dominated by the middle rare-earth elements Pr, Dy, Tb, and Gd together with Ge. Factor 4 (Rb, K_2O, Ba, Li, and W) is the region's principal potassic/hydrothermal-affinity signature. Factor 5 (CaO, Sr, and MgO, opposed by SiO_2) is a calcic/carbonate mineralogical component. Factor 6 shows an inverse relationship between TiO_2 and Cr (both negative) and Mo (positive), with secondary contributions from Cs, Pb, Co, and Se , the

region's principal Mo-bearing association. Factor 7 is a comparatively weak, diffuse association of Y, Hg, Zr, Nb, Th, and Ba (all below the 0.50 interpretive threshold). Factor 8 is dominated by a negative Ta–W association opposed by a weaker positive Au–Cd–Ag assemblage. These eight factors , in particular the detrital REE–U–Hf–Zr–Ta provenance signature (Factor 1) and the potassic/hydrothermal signature (Factor 4) , constitute the regional framework against which the jarosite-domain geochemistry is tested in Section 4.9.

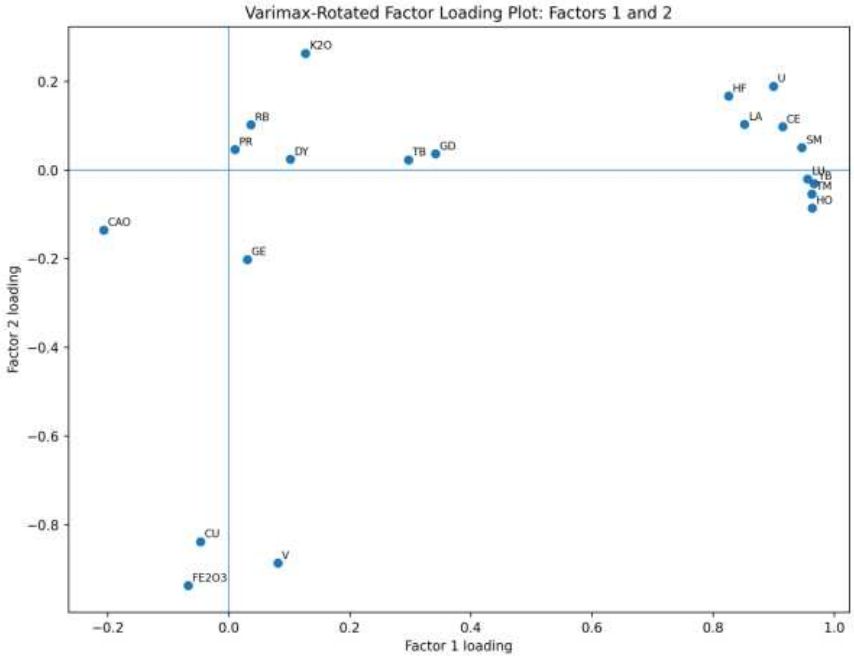


Fig. 5. Varimax-rotated factor loading plot for Factors 1 and 2.

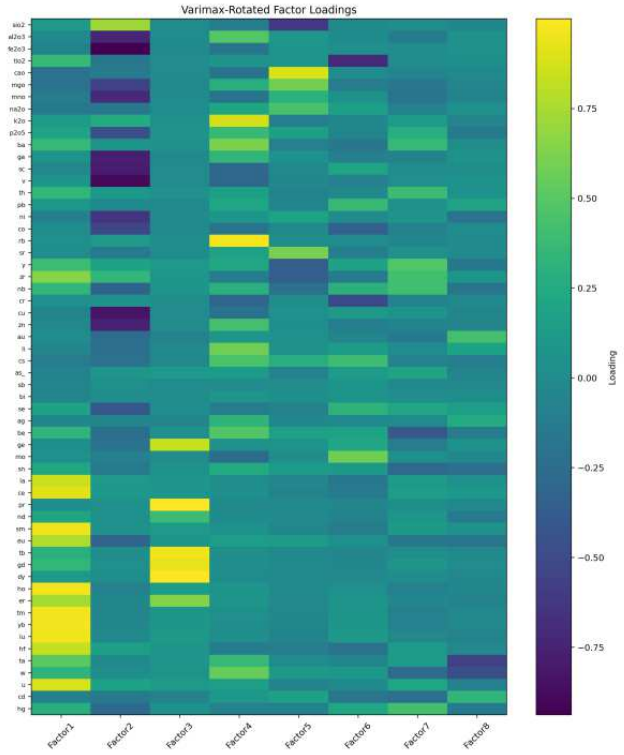


Fig. 6. Varimax-rotated factor-loading heatmap for the eight-factor regional solution.

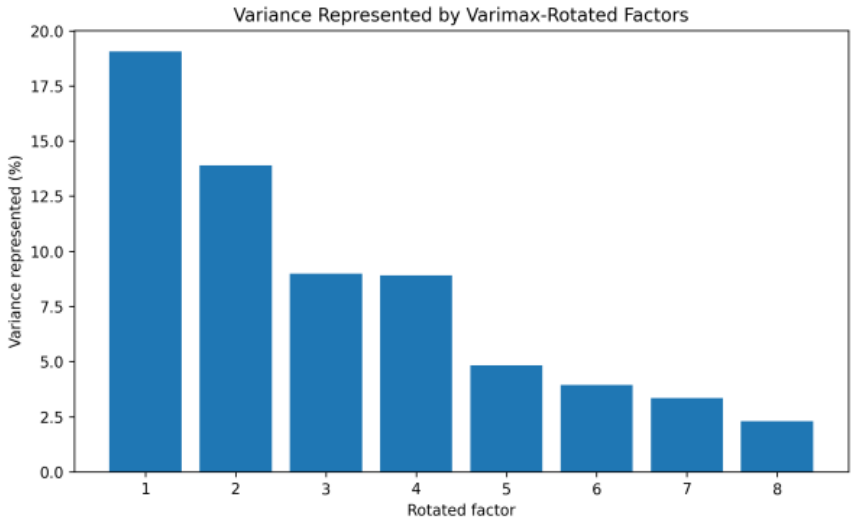


Fig. 7. Percentage of variance represented by each Varimax-rotated regional factor.

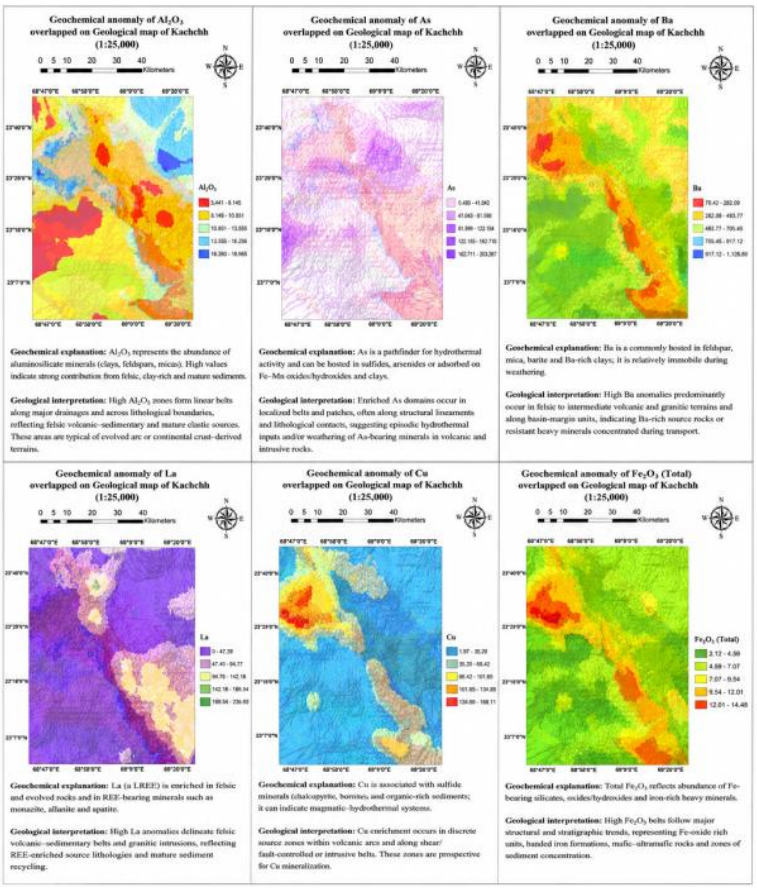


Fig. 8. Anomaly maps of Al_2O_3, As, Ba, La, Cu, and total Fe_2O_3 overlain on the 1:25,000 geological map of the study area.

4.5 Regional single-element anomaly maps

Anomaly maps of thirteen major and trace elements (Al_2O_3, As, Ba, La, Cu, total Fe_2O_3, Ni, SiO_2, Th, U, V, Zn, and Zr) were overlain on the 1:25,000 geological map (Fig. 8, Fig. 9). Al_2O_3 anomalies reflect the abundance of aluminosilicate minerals (clays, feldspars, micas) and high values indicate

strong contribution from felsic, clay-rich, and mature sediments. As acts as a pathfinder for hydrothermal activity, being hosted in sulfides, arsenides, or adsorbed on Fe–Mn oxides/hydroxides and clays. Ba is commonly hosted in feldspar, mica, and Ba-rich clays. La, Th, and Zr are enriched in felsic and evolved rocks and in resistant accessory minerals (monazite, allanite, zircon). Cu is associated with sulfide minerals and can indicate magmatic–hydrothermal systems. Total Fe_2O_3 reflects Fe-bearing silicates, oxides/hydroxides, and iron-rich heavy minerals. Ni and V are associated with mafic–ultramafic rocks and Fe–Ti oxides. SiO_2 reflects quartz-rich lithologies. U occurs in uraninite, coffinite, phosphates, and organic-rich sediments under reducing conditions. Zn is linked to sphalerite and carbonate-rich sediments and, with Cu and Pb, suggests potential polymetallic mineralization.

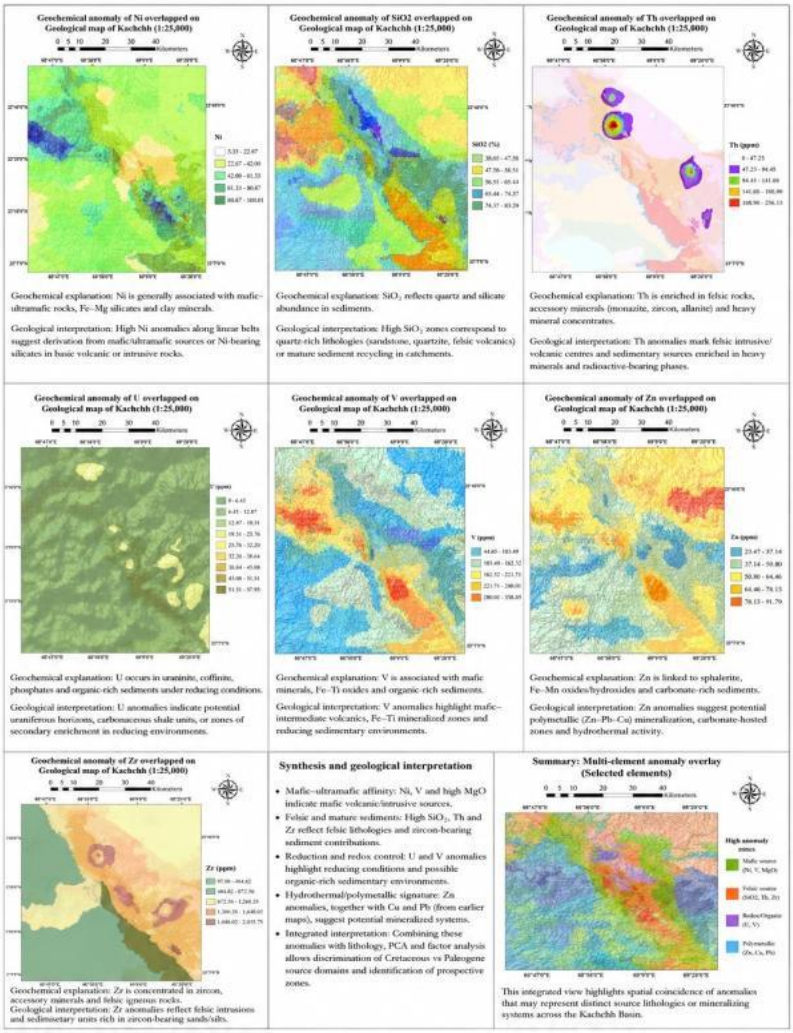


Fig. 9. Anomaly maps of Ni, SiO_2, Th, U, V, and Zn, together with a Zr anomaly map, overlain on the 1:25,000 geological map, and a synthesis panel integrating the multi-element geochemical framework for the Kachchh study area.

Considered jointly, this thirteen-element anomaly framework resolves four broad regional geochemical associations: (i) a mafic–ultramafic affinity (Ni, V, MgO); (ii) a felsic/mature-sediment affinity (SiO_2, Th, Zr); (iii) a reduction/redox-control affinity (U, V); and (iv) a hydrothermal/polymetallic affinity (Zn, Cu, As). These correspond closely to the lithological (Factor 2), provenance (Factors 1 and 3), and hydrothermal/chalcophile (Factors 4, 6, 8) assemblages resolved independently by the factor analysis (Section 4.4).

4.6 PCA-based regional multivariate anomaly assessment

A PCA-based anomaly plot was prepared using the PC1 and PC2 scores (Fig. 10); samples within the upper 5% of the PC1–PC2 radial distance distribution (threshold = 7.98) were flagged as multivariate PCA anomalies.

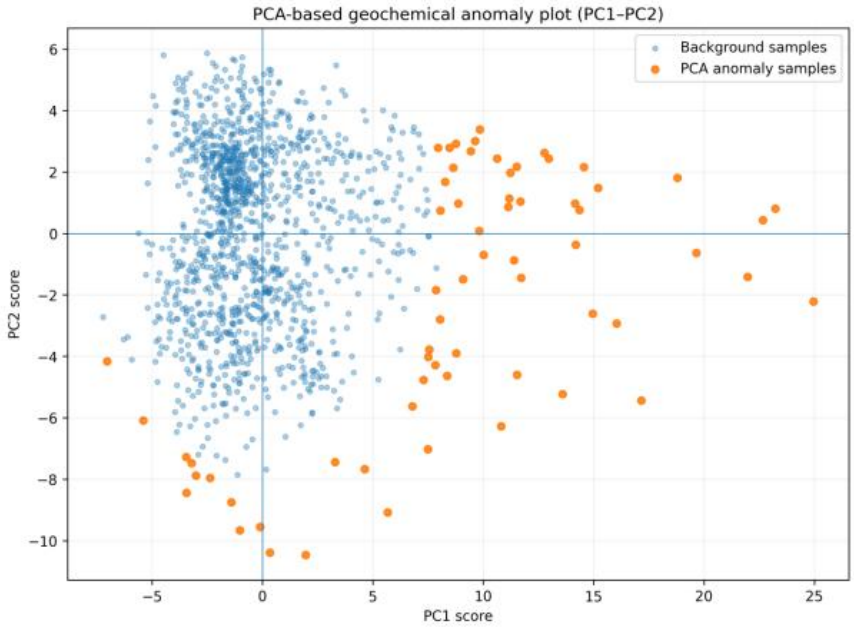


Fig. 10. PCA-based geochemical anomaly plot for the regional dataset. Samples in the upper 5% of the radial PC1–PC2 distance distribution are highlighted as multivariate PCA anomalies.

4.7 Regional factor-analysis spatial anomaly integration

The factor-score maps were integrated with the mapped geological framework (Fig. 11). MgO, Fe_2O_3, V, Ni, Cu, Zn, Sc, and Ga are relatively elevated mainly in the central to south-eastern parts of the study area, consistent with Factor 2, while SiO_2 defines broad, spatially complementary belts. La, Th, and Zr anomalies occur as localized, spatially coherent centres consistent with Factor 1 and resistant accessory-mineral concentration. None of the mapped regional Factor 4 (potassic) or Factor 6 (Ti–Cr–Mo) anomaly domains coincide spatially with the Matanomadh jarosite locality at the resolution of the regional survey, a point revisited in Section 5.3.

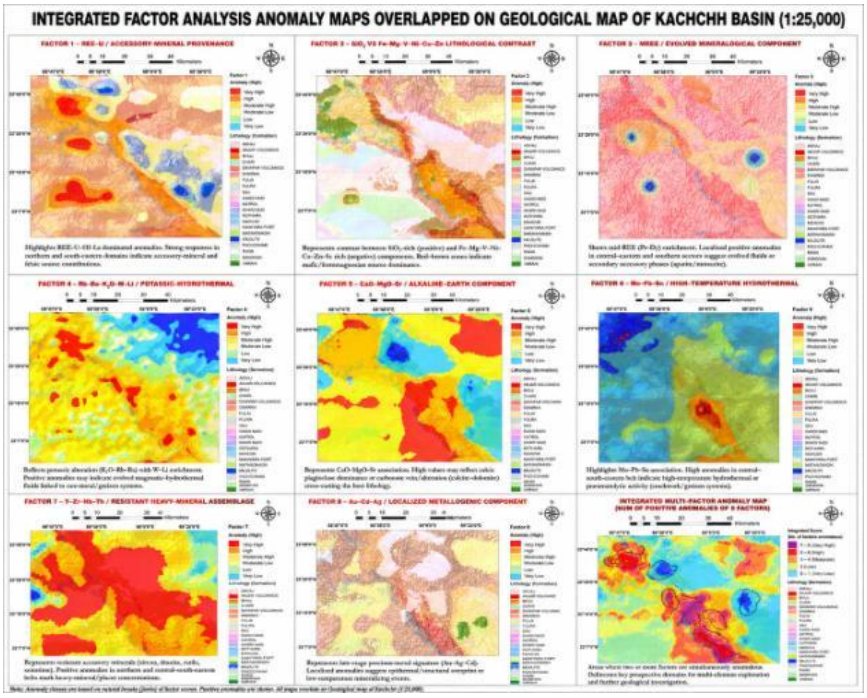


Fig. 11. Integrated factor-analysis anomaly maps overlain on the geological map of the Kachchh Basin (1:25,000).

4.8 Jarosite-domain geochemistry (PM-JAR samples)

The jarosite-bearing domain at Matanomadh was sampled in two stages: an initial 15 samples (PM-JAR-01 to PM-JAR-15) analysed for Fe_2O_3, SO_3, K_2O, Al_2O_3, Mo, As, U, and Th, and a further 15 samples (PM-JAR-16 to PM-JAR-30) from the same domain, analysed by XRF for major oxides (including SiO_2) and by ICP-MS for an extended trace-element suite (Mo, As, Sb, Se, U, Th, Pb, Cu, Zr). Combining both stages, the domain shows Fe_2O_3 ranging from 29.8 to 45.2 wt.% (n = 30) and SO_3 from 8.4 to 31.8 wt.% (n = 30), consistent with an Fe-sulfate-rich mineral assemblage (Rye and Alpers, 1997; Cruells and Roca, 2022). The spatial distribution of SO_3 and Fe_2O_3 across the sampled jarosite domain is shown in Fig. 12. K_2O ranges from 1.8 to 5.5 wt.%, while Al_2O_3 shows an inverse pattern (1.8–14.5 wt.%). Mo (78–951 ppm, n = 30) and As (0–390 ppm, n = 30) are both highly variable. The second-stage samples additionally show SiO_2 ranging from 5.5 to 22.4 wt.% (n = 15), markedly lower than typical regional sediment, and a coherent chalcophile/pathfinder suite , Sb (1.7–36.0 ppm), Se (8.9–53.9 ppm), Pb (15.6–118.6 ppm), and Cu (34.9–162.5 ppm) , together with Zr (5.8–32.2 ppm, n = 15), markedly lower than typical regional sediment. Because the jarosite sub-dataset remains modest in size (n = 30 for the core variables, n = 15 for the extended suite), these internal ranges should be regarded as indicative of a coherent geochemical pattern rather than as exhaustively representative of the full domain.

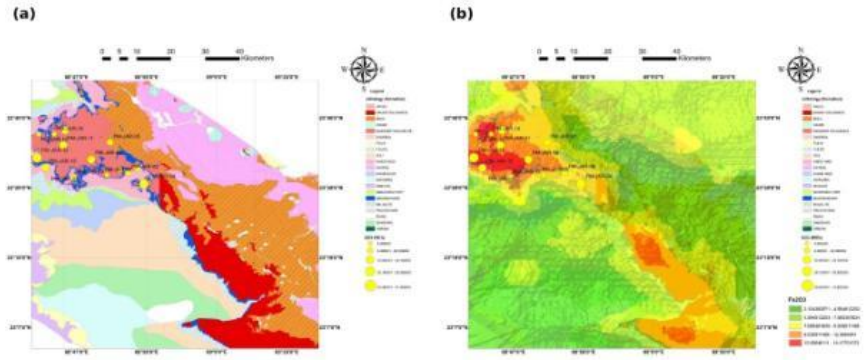


Fig. 12. Spatial distribution of jarosite-related geochemical anomalies at Matanomadh: (a) SO_3 (wt.%) by graduated sample symbols, and (b) interpolated Fe_2O_3 anomaly map.

Variable	Local background range	Local BG median	Jarosite-domain range (n)	Jarosite median	EF (median ratio)
Fe_2O_3 (wt.%)	3.53 – 10.82	7.72	29.80 – 45.20 (30)	38.00	4.92
K_2O (wt.%)	0.54 – 2.68	1.08	1.80 – 5.50 (30)	4.05	3.77
Al_2O_3 (wt.%)	8.28 – 14.90	10.31	1.80 – 14.50 (30)	5.65	0.55
SiO_2 (wt.%)	50.89 – 73.39	62.05	5.50 – 22.40 (15)	12.10	0.20
Mo (ppm)	1.91 – 37.87	15.61	78.0 – 951.0 (30)	297.50	19.06
As (ppm)	5.01 – 84.67	40.19	0.0 – 390.0 (30)	122.50	3.05
Sb (ppm)	0.04 – 0.89	0.25	1.70 – 36.00 (15)	9.90	39.60
Se (ppm)	0.20 – 2.45	0.73	8.90 – 53.90 (15)	25.00	34.01
U (ppm)	0.18 – 5.13	1.67	0.60 – 2.50 (30)	1.65	0.99
Th (ppm)	6.00 – 128.00	7.00	0.20 – 0.70 (30)	0.41	0.06
Pb (ppm)	16.00 – 59.00	20.50	15.60 – 118.60 (15)	55.80	2.72
Cu (ppm)	13.00 – 134.00	47.00	34.90 – 162.50 (15)	98.20	2.09
Zr (ppm)	180.00 – 2252.00	513.00	5.80 – 32.20 (15)	20.30	0.04

Table 3. Jarosite-domain geochemistry compared with the local stream-sediment background defined by the 20 nearest regional samples (all within 5.4 km of the jarosite-domain centroid). n given in parentheses; SO_3 has no regional-survey benchmark (not analysed regionally) and is reported in Section 4.8 only.

4.9 Jarosite domain versus local stream-sediment background

To place the jarosite-domain geochemistry (Section 4.8) in the context of its immediate surroundings, the 20 nearest regional stream-sediment samples (all within 5.4 km of the jarosite-domain centroid; Section 3.8) were extracted and compared with the jarosite domain for thirteen variables (Table 3): eight at n = 30 (Fe_2O_3, K_2O, Al_2O_3, Mo, As, U, Th, plus SO_3 which has no regional benchmark) and six at n = 15, PM-JAR-16–30 only (SiO_2, Sb, Se, Pb, Cu, Zr). The jarosite domain is enriched relative to the local background median by a factor of approximately 4.9 for Fe_2O_3, 3.8 for K_2O, 19.1 for Mo, 3.1 for As, 39.6 for Sb, 34.0 for Se, 2.7 for Pb, and 2.1 for Cu, but is depleted by a factor of approximately 0.55 for Al_2O_3, 0.20 for SiO_2, and, most markedly, 0.06 for Th and 0.04 for Zr , both one to two orders of magnitude below the local background median. U shows no net enrichment relative to the local background (≈ 0.99×).

This pattern is interpreted in detail in Section 5.3. In brief, the pronounced Th and Zr depletion, together with the SiO_2 depletion, indicate that the jarosite domain is neither a locally exhumed fragment of the region's typical detrital lithology nor simply a silicate sediment overprinted by alteration, while the strong, locally exceeding Fe–K–Mo–As–Sb–Se–Pb–Cu enrichment indicates a coherent, authigenic, in-situ geochemical process superimposed on that detrital background.

5. Discussion

5.1 The regional detrital and lithological framework

Factor 1 (heavy-to-light REE, U, Hf, Zr, Ta) and Factor 2 (Fe_2O_3–V–Cu–Sc–Ga–Zn–Al_2O_3–MnO–Ni–MgO versus SiO_2) together define the two dominant axes of regional geochemical variability, representing, respectively, a resistant accessory-mineral/felsic-provenance signature and a silica-rich versus Fe–Mg-rich lithological contrast. Factor 3, a second and geochemically distinct middle-REE–Ge association, and Factor 7, a weak, diffuse Y–Hg–Zr–Nb–Th association, provide subordinate expressions of accessory-mineral control. These associations, together with the single-element anomaly framework (Section 4.5), establish the region's dominant detrital and lithological geochemical background, against which the Matanomadh jarosite domain is tested in Section 5.3.

5.2 The regional hydrothermal-affinity and subordinate factors

Factor 4 (Rb–K_2O–Ba–Li–W) is the region's principal potassic/hydrothermal-affinity signature, plausibly reflecting K-feldspar enrichment, sericitic alteration, or a more evolved fluid component associated with rare-metal or greisen-type systems elsewhere in the basin. Factor 5 (CaO–Sr–MgO, opposed by SiO_2) represents an independent calcic/carbonate component. Factor 6, an inverse TiO_2–Cr versus Mo(–Cs–Pb–Se) association, is the region's principal Mo-bearing signature, potentially

reflecting a specialized hydrothermal or pneumatolytic overprint distinct from the primary mafic Ti–Cr-bearing accessory-oxide assemblage. Factor 8 (negative Ta–W opposed by weak positive Au–Cd–Ag) is a minor, localized association. None of these factors, on the evidence of the regional factor-score maps (Section 4.7), forms a spatially coherent anomaly domain coincident with the Matanomadh jarosite locality.

5.3 Testing jarosite genesis against the regional framework

The central question motivating this study is whether the Matanomadh jarosite domain's geochemistry is embedded within, or decoupled from, the regional detrital-provenance and hydrothermal-affinity framework established in Sections 5.1–5.2, and what this implies for the debate between an ancient, possibly volcanogenic-hydrothermal Paleocene origin (Dharaiya et al., 2025) and an ongoing, supergene, pyrite-oxidation-driven origin (Guha et al., 2026). With the expanded 30-sample jarosite dataset, four independent lines of geochemical evidence now bear on this question.

First, the jarosite domain shows pronounced Th and Zr depletion relative to the local stream-sediment background (≈ 0.06× and ≈ 0.04× the local median, respectively; Table 3), together with no local enrichment in U (≈ 0.99×) and no inheritance of the region's dominant REE–U–Hf–Zr–Ta detrital-provenance signature (Factor 1/PC1). Because Th and Zr are hosted overwhelmingly in resistant detrital accessory minerals (zircon, monazite, allanite) throughout the regional dataset (Section 5.1), their near-total absence from the jarosite domain , Zr depleted even more severely than Th , indicates that this domain is not simply a locally exhumed or concentrated fragment of the region's typical detrital lithology. This is more consistent with an authigenic, chemically precipitated Fe–S–K mineral phase than with a fossil hydrothermal-alteration halo developed within, and inheriting the detrital signature of, the region's clastic host rocks.

Second, the jarosite domain is markedly depleted in SiO_2 relative to the local background (≈ 0.20× the local median), indicating that the domain is not simply an ordinary quartzo-feldspathic sediment carrying a secondary Fe-sulfate overprint, but is dominated by non-silicate, Fe-sulfate mineralogy essentially undiluted by detrital quartz and feldspar. Combined with the Th–Zr depletion, this SiO_2 depletion reinforces the case that the jarosite domain represents an authigenic mineral concentration rather than an altered clastic sediment.

Third, the jarosite domain is strongly enriched relative to the local background in Fe_2O_3 (≈ 4.9×), Mo (≈ 19.1×), As (≈ 3.1×), Sb (≈ 39.6×), Se (≈ 34.0×), Pb (≈ 2.7×), and Cu (≈ 2.1×), while Al_2O_3 is depleted (≈ 0.55×). This coupled chalcophile/pathfinder-element enrichment , particularly the very strong Sb and Se enrichment, in addition to the previously noted Mo and As , is consistent with the well-documented capacity of Fe(III)-oxyhydroxysulfate phases, including jarosite itself, to scavenge

chalcophile and oxyanion-forming trace elements from pore fluids during low-temperature precipitation, either by surface adsorption or by structural substitution for sulfate (Savage et al., 2005; Cruells and Roca, 2022) , a process that operates effectively under near-surface, low-temperature, oxidizing conditions and does not require a distinct high-temperature hydrothermal fluid source. The magnitude of the Sb and Se enrichment in particular is more consistent with the kind of trace-element scavenging documented in modern acid-sulfate weathering and acid-mine-drainage-type Fe-oxyhydroxysulfate systems than with a single ancient hydrothermal pulse.
Fourth, although the jarosite domain shows strong K_2O enrichment relative to the local background (≈ 3.8×), this cannot be straightforwardly attributed to the same process responsible for the region's independent potassic-hydrothermal signature (Factor 4: Rb–K_2O–Ba–Li–W). The regional factor-score maps show no coincidence between the mapped Factor 4 anomaly domains and the Matanomadh locality (Section 4.7), and, critically, potassium is a structural constituent of jarosite itself , occupying the mineral's A-site, with documented natrojarosite–natroalunite solid solutions at this locality indicating partial Na substitution for K (Guha et al., 2026) , so elevated K_2O in the jarosite domain is more parsimoniously explained as a direct mineralogical consequence of jarosite abundance than as evidence of a regional K-metasomatic or hydrothermal fluid event. The Rb, Ba, Li, and W enrichment that characterizes the region's Factor 4 elsewhere in the basin is notably absent from the reported jarosite-domain analytical suite and cannot be evaluated directly, which is acknowledged as a limitation in Section 5.6.
Taken together, these four lines of evidence , detrital/REE decoupling with severe Th and Zr depletion, SiO_2 depletion indicating a non-detrital mineralogy, coupled Fe–Mo–As–Sb–Se–Pb–Cu enrichment consistent with low-temperature Fe-oxyhydroxysulfate scavenging, and a mineralogically parsimonious (rather than regionally hydrothermal) explanation for the K_2O enrichment , provide an independent, basin-scale geochemical line of evidence consistent with the ongoing, supergene, pyrite-oxidation-driven origin recently proposed for the western Kutch jarosite assemblage on isotopic and mineralogical grounds (Guha et al., 2026), and do not require invoking a genetically distinct Paleocene volcanogenic-hydrothermal fluid event as speculated by earlier workers (Dharaiya et al., 2025). This conclusion should be regarded as a complementary, regional-scale corroboration of the isotopic and mineralogical case rather than an independent proof: the present regional stream-sediment survey did not measure SO_3 or sulfur isotopes, and the original jarosite-domain dataset does not include Rb, Ba, Li, or W, so a direct multivariate test of the jarosite domain against the full eight-factor regional structure was not possible (Section 5.6).

5.4 Compositional-data sensitivity analysis

Because stream-sediment geochemical data are compositional (Aitchison, 1986; Filzmoser et al., 2009a, 2009b; Reimann et al., 2012), a sensitivity analysis was performed by converting all major-oxide concentrations to a common ppm basis, replacing recorded zero values with 65% of the minimum positive value recorded for each variable (Martin–Fernández et al., 2003), applying a centred log-ratio (clr) transformation, and re-running PCA on the regional dataset. The clr-transformed PCA yielded 12 components explaining 77.97% of total variance, closely comparable to the untransformed analysis (77.47%). Critically, clr-PC1 remains dominated by the same coherent REE suite (Sm, Ce, Gd, Tb, Er, Lu, Ho, Yb) opposed by MgO, Al_2O_3, Zn, Fe_2O_3, MnO, Na_2O, Ga, and Ni, confirming that the primary REE-versus-mafic-element contrast underlying Factor 1/PC1 , the detrital-provenance signature used as the basis for the decoupling argument in Section 5.3 , is not an artefact of data closure. The secondary structure reorganizes under the closure correction, with clr-PC2 dominated by a K_2O–Rb–Y–Th–SiO_2–Zr–As–Ba assemblage rather than reproducing the untransformed silica-versus-mafic contrast, indicating that the region's potassic/hydrothermal signature (Factor 4) becomes proportionally more prominent once closure is corrected; this does not alter the Section 5.3 conclusion, since that argument rests on the Th/Zr/REE-depletion evidence (robust to closure) rather than on the potassic factor.

5.5 Wider implications

For regional exploration and provenance studies independent of the jarosite question, the detrital lithological (Factor 2/PC2) and provenance (Factor 1/PC1) framework established here provides a basis for discriminating source-rock domains across the Kachchh Mainland, and the region's subordinate hydrothermal-affinity (Factor 4) and Mo-bearing (Factor 6) associations warrant follow-up field evaluation where they coincide spatially with structural features. For Mars-analog research, the finding that the Matanomadh jarosite domain is geochemically decoupled from the region's detrital sediment framework is itself of interest: it indicates that this terrestrial jarosite occurrence records a comparatively “clean” local aqueous-alteration signature largely unaffected by detrital dilution from the surrounding catchment, which may make it a more faithful analog for interpreting the geochemistry of in-situ jarosite deposits on Mars than a jarosite occurrence embedded within a mixed detrital sedimentary sequence would be.

5.6 Methodological limitations

Several limitations qualify the conclusions of this study. The core jarosite-domain interpretation (Sections 4.8–4.9, 5.3) combines two sampling stages with only partially overlapping analytical suites: the original 15 samples do not include SiO_2, Sb, Se, Pb, Cu, or Zr, and neither stage includes

Rb, Ba, Li, or W, so a direct multivariate comparison of the jarosite domain against the full eight-factor regional structure, and a direct test of whether the region's Rb–Ba–Li–W potassic signature extends into the jarosite domain, remains impossible. Sulfur-isotope data, which provided the most decisive evidence in the recent mineralogical literature (Guha et al., 2026), were not available for either dataset used here. The local-background comparison (Section 3.8, Table 3) is based on the 20 nearest regional samples within a 5.4 km radius and assumes that this radius adequately represents the immediate geochemical surroundings of the jarosite domain; a denser, purpose-designed sampling grid around the Matanomadh locality, analysed for the same variable suite as the regional survey, would allow a more rigorous test of the conclusions reached here. A preliminary A-site (K–Na–H_3O) speciation assessment for the jarosite-group minerals was also considered for inclusion in this study but is omitted pending a fully documented analytical method (e.g., electron-microprobe or Rietveld-refinement data), since site-occupancy classification cannot be responsibly reported without a stated basis; this is recommended as a priority for follow-up mineralogical work at this locality. Finally, all genetic interpretations offered in this study are geochemical hypotheses consistent with, but not independently proving, the supergene origin proposed on isotopic grounds; they should be evaluated alongside continued mineralogical, isotopic, and field-based investigation of the Matanomadh occurrence.

6. Conclusions

A 1,295-sample, 58-variable regional stream-sediment geochemical survey of the Kachchh Mainland resolves a well-defined detrital and lithological framework (KMO = 0.880; Bartlett's χ^2 = 120,039.46, $p < 0.001$; 12 PCA components explaining 77.47% of variance; an eight-factor Varimax solution), dominated by a REE–U–Hf–Zr–Ta provenance signature (Factor 1/PC1) and a silica-versus-mafic lithological contrast (Factor 2/PC2), with subordinate potassic-hydrothermal (Factor 4) and Ti–Cr–Mo (Factor 6) associations.

Relative to the 20 nearest regional stream-sediment samples, the expanded Matanomadh jarosite domain (n = 30 for core variables; n = 15 for an extended trace-element suite) is strongly enriched in Fe_2O_3 (≈ 4.9× local median), K_2O (≈ 3.8×), Mo (≈ 19.1×), As (≈ 3.1×), Sb (≈ 39.6×), Se (≈ 34.0×), Pb (≈ 2.7×), and Cu (≈ 2.1×); depleted in Al_2O_3 (≈ 0.55×) and SiO_2 (≈ 0.20×); and markedly depleted in Th (≈ 0.06×) and Zr (≈ 0.04×), with no net enrichment in U.

This pattern indicates that the jarosite domain does not inherit the region's dominant detrital REE–Th–Zr provenance signature or its bulk silicate sediment character, and is compositionally decoupled from the basin's principal lithological and hydrothermal-affinity factors, consistent with an authigenic, in-situ Fe–S–K mineral phase whose Mo–As–Sb–Se–Pb–Cu enrichment reflects pathfinder- and chalcophile-element scavenging during low-temperature Fe-oxyhydroxysulfate

precipitation, and whose K_2O content is more parsimoniously explained by the jarosite crystal structure itself than by the region's independent potassic-hydrothermal factor.

These basin-scale geochemical observations provide an independent line of evidence consistent with the ongoing, supergene, pyrite-oxidation-driven origin recently proposed for the western Kutch jarosite assemblage on isotopic and mineralogical grounds (Guha et al., 2026), complementing rather than superseding that outcrop-scale evidence, and do not require a genetically distinct Paleocene volcanogenic-hydrothermal fluid source as previously speculated (Dharaiya et al., 2025).

The regional-versus-local geochemical framework demonstrated here , combining regional factor/PCA analysis with a nearest-neighbour local-background comparison , is transferable to testing the origin of other localized secondary-mineral or alteration anomalies within the Kachchh Basin and comparable regional stream-sediment datasets elsewhere.

Before submission, the compositional nature of the geochemical data should be finally addressed (Section 5.4), the analytical methodology for both jarosite-domain sampling stages should be fully documented (Section 3.1), the two analytical suites should ideally be harmonized (all 30 samples analysed for the full variable set), and a documented A-site speciation study should be completed before any mineral-structural site-occupancy claims are incorporated.

Declarations

Funding

There was no external funding has been provided from any organization

Conflicts of interest

The authors declare no conflict of interest.

Acknowledgements

The authors are thankful to anonymous reviewers for their critical but constructive comments which improved the quality of the manuscript. Analytical facilities at IISER Kolkata XRF are gratefully acknowledged. We thank faculty and students of K.S.K.V. Kachchh University for logistical support during fieldwork.

References

1. Aitchison, J., 1986. The Statistical Analysis of Compositional Data. Chapman & Hall, London.
2. Bhattacharya, S., Mitra, S., Gupta, S., Jain, N., Chauhan, P., Parthasarathy, G., Ajai, 2016. Jarosite occurrence in the Deccan Volcanic Province of Kachchh, western India: spectroscopic studies on a Martian analog locality. Journal of Geophysical Research: Planets 121, 402–431.

3. Biswas, S.K., 1992. Tertiary stratigraphy of Kutch. Journal of the Palaeontological Society of India 37, 1–29.
4. Biswas, S.K., 2005. A review of structure and tectonics of Kutch basin, western India, with special reference to earthquakes. Current Science 88(10), 1592–1600.
5. Chauhan, G., Biswas, S.K., Thakkar, M.G., Page, K.N., 2021. The unique geoheritage of the Kachchh (Kutch) Basin, western India, and its conservation. Geoheritage 13, 1–34.
6. Chitale, D.V., 1987. Natroalunite in a laterite profile over Deccan Trap basalts at Matanumad, Kutch, India. Clays and Clay Minerals 35(3).
7. Cruells, M., Roca, A., 2022. Jarosites: formation, structure, reactivity and environmental applications. Metals 12(5), 802.
8. Dharaiya, A.N., Gaikwad, S.K., Sangode, S.J., Thakkar, M.G., Singh, R., 2025. Petrogenesis of Palaeocene jarosite at Matanomadh, Kachchh, western India: analog for Martian environments. Journal of the Geological Society of India 101(8), 1213–1223.
9. Dutta, S., Mathews, R.P., Singh, B.D., Tripathi, S.M., Singh, A., Saraswati, P.K., Banerjee, S., Mann, U., 2011. Petrology, palynology and organic geochemistry of Eocene lignite of Matanomadh, Kutch Basin, western India: implications to depositional environment and hydrocarbon source potential. International Journal of Coal Geology 85(1), 91–102.
10. Farrand, W.H., Glotch, T.D., Rice, J.W., Hurowitz, J.A., Swayze, G.A., 2009. Discovery of jarosite within the Mawrth Vallis region of Mars: implications for the geologic history of the region. Icarus 204(2), 478–488.
11. Filzmoser, P., Hron, K., Reimann, C., 2009a. Principal component analysis for compositional data with outliers. Environmetrics 20, 621–632.
12. Filzmoser, P., Hron, K., Reimann, C., Garrett, R., 2009b. Robust factor analysis for compositional data. Computational Statistics & Data Analysis 53(9), 3096–3107.
13. Guha, S., Acharya, S.S., Panigrahi, M.K., 2026. Multiproxy evidence for natrojarosite–natroalunite solid solutions in western Kutch: jarosite formation, preservation, and Martian implications. Journal of Geophysical Research: Planets 131, e2025JE009601.
14. Helba, H., et al., 2021. Stream sediment geochemical exploration for gold in Central Eastern Desert, Egypt: application of the concentration-number fractal model, factor analysis, and geochemical mineralization probability index. Geochemistry 81(4).
15. Malik, J.N., Srivastava, E., Gadhavi, M.S., Livio, F., Sharma, N., Arora, S., Parrino, N., Burrato, P., Sulli, A., 2024. Holocene surface-rupturing paleo-earthquakes along the Kachchh Mainland Fault: shaping the seismic landscape of Kachchh, western India. Scientific Reports 14, 1–17.
16. Mandal, S., et al., 2023. Deep seismic reflection imaging of Mesozoic Kachchh rift, NW India: implications for evolution. Tectonics 42, e2023TC007992.

17. Martin–Fernández, J.A., Barceló-Vidal, C., Pawlowsky-Glahn, V., 2003. Dealing with zeros and missing values in compositional data sets using nonparametric imputation. Mathematical Geology 35(3), 253–278.
18. Nazarpour, A., et al., 2022. Application of geographically weighted regression (GWR) and singularity analysis to identify stream sediment geochemical anomalies, case study, Takab area, NW Iran. Journal of Geochemical Exploration.
19. Rai, A.K., et al., 2026. R-mode factor analysis of stream sediment geochemical data: a multivariate statistical approach for critical mineral exploration in the Bundelkhand Craton, India. Geosystems and Geoenvironment.
20. Reimann, C., Filzmoser, P., Garrett, R.G., 2002. Factor analysis applied to regional geochemical data: problems and possibilities. Applied Geochemistry 17, 185–206.
21. Reimann, C., Filzmoser, P., Garrett, R.G., Dutter, R., 2012. Statistical Data Analysis Explained: Applied Environmental Statistics with R, 2nd ed. Wiley.
22. Rye, R.O., Alpers, C.N., 1997. The stable isotope geochemistry of jarosite. U.S. Geological Survey Open-File Report 97-88.
23. Savage, K.S., Bird, D.K., O'Day, P.A., 2005. Arsenic speciation in synthetic jarosite. Chemical Geology 215, 473–498.
24. Shine, Y.J., et al., 2022. Generation of geochemical exploration targets from regional stream sediment data using Principal Component and Factor Analysis. Tanzania Journal of Science.
25. Srivastava, V.K., Singh, B.P., 2017. Shoreface to estuarine sedimentation in the late Paleocene Matanomadh Formation, Kachchh, western India. Journal of Asian Earth Sciences 136, 1–15.